Journal of Maps

ISSN: 1744-5647 (Online) Journal homepage: www.tandfonline.com/journals/tjom20

A deep-seated roto-translational landslide in flysch rocks in the Northern Apennines (the Casale-Colla landslide, Ferriere, Italy)

Cecilia Fabbiani , Marco Mulas , Vincenzo Critelli , Irene Ghiselli , Jean Pascal Iannacone , Francesco Lelli , Melissa Tondo , Giovanni Truffelli & Alessandro Corsini

To cite this article: Cecilia Fabbiani , Marco Mulas , Vincenzo Critelli , Irene Ghiselli , Jean Pascal Iannacone , Francesco Lelli , Melissa Tondo , Giovanni Truffelli & Alessandro Corsini (2026) A deep-seated roto-translational landslide in flysch rocks in the Northern Apennines (the Casale-Colla landslide, Ferriere, Italy), Journal of Maps, 22:1, 2693615, DOI: 10.1080/17445647.2026.2693615

To link to this article: https://doi.org/10.1080/17445647.2026.2693615

Published online: 23 Jul 2026.

JOURNAL OF MAPS
2026, VOL. 22, NO. 1, 2693615
https://doi.org/10.1080/17445647.2026.2693615

Taylor & Francis
by informa

OPEN ACCESS Check for updates

A deep-seated roto-translational landslide in flysch rocks in the Northern Apennines (the Casale-Colla landslide, Ferriere, Italy)

Cecilia Fabbiani[a], Marco Mulas[a], Vincenzo Critelli[a], Irene Ghiselli[b], Jean Pascal Iannacone[c], Francesco Lelli[a], Melissa Tondo[a], Giovanni Truffelli[b] and Alessandro Corsini[a]

[a]Department of Chemical and Geological Sciences, University of Modena and Reggio Emilia, Modena, Italy; [b]Emilia-Romagna Region, Agency for Territorial Security and Civil Protection, Piacenza, Italy; [c]External Consultant, Modena, Italy

ABSTRACT
This study presents a detailed map and reference cross-sections of the Casale-Colla landslide in the Northern Apennines (Municipality of Ferriere, Province of Piacenza, Italy). It is an active deep-seated roto-translational slide in flysch rock masses causing significant damage to roads and hamlets. The map results from a comprehensive geological and geomorphological characterization supported by multitemporal aerial images, high resolution digital terrain models, displacement monitoring, boreholes and geophysics. The map and the cross-sections show that the landslide comprises five main sub-units, controlled by multiple sliding surfaces extending to a depth of 40 m. Monitoring data indicate that landslide velocity decreases from the upper to the lower sub-units, suggesting overthrusts between them, that the landslide comprises five main sub-units. The results demonstrate the added-value of integrating conventional investigations and remote-sensing datasets for the analysing and mapping of complex deep-seated slope instabilities.

ARTICLE HISTORY
Received 19 November 2025
Revised 11 June 2026
Accepted 12 June 2026

KEYWORDS
Deep-seated landslides; Northern Apennines; mapping; monitoring; risk zoning

Key policy highlights

- The map identifies five landslide sub-units with distinct kinematics, providing an immediate basis for risk zoning and land-use regulation.
- Monitoring data show decreasing displacement rates downslope, supporting prioritisation of mitigation in the most active upper sectors.
- The map and the cross-sections produced for the Casale-Colla landslide offer a reliable geological framework to guide stabilization works and the protection of critical infrastructure, including the SS654 road.
- The correlation between rainfall and movement rates revealed by this study offers in perspective the opportunity to develop rainfall-based early-warning thresholds.

1. Introduction

Geomorphological mapping is a fundamental tool for reconstructing and representing the spatiotemporal evolution of landslides and assessing their hazard (Carrara et al., 2003; Chelli et al., 2021; Guzzetti et al., 2012; Lee, 2001). Several studies have provided detailed maps and spatial delineations of landslides (Bozzano et al., 2020; Bucci et al., 2021; Bufalini et al., 2021; Chelli et al., 2016; Dotta et al., 2023; Fioraso, 2017; Giacomelli et al., 2021; Santangelo et al., 2021). The usage of integrated investigation and monitoring approaches is common in deep-seated rock sliding phenomena (Agliardi et al., 2001; Corsini et al., 2015). High-resolution Digital Elevation Models (DEMs) derived from Light Detection and Ranging (LiDAR) can be used to capture fine-scale morphological features and accurately define landslide boundaries (Ciccarese et al., 2024; Devoto et al., 2020; Jaboyedoff et al., 2012; Johnson et al., 2023; Lelli et al., 2025; Pawluszek, 2019; Pellicani et al., 2019; Sterzai et al., 2010). Displacement rates can be analysed through the integration of ground-based monitoring systems, such as continuous global navigation systems receivers (C-GNSS) (Cenni et al., 2021; Mantovani et al., 2022; Mulas et al., 2020a, 2020b), and other remote sensing techniques, including Multi-Temporal SAR Interferometry (MT-InSAR) (Bozzano et al., 2017; Ciuffi et al., 2024; Mondini et al., 2021; Scaioni et al., 2014; Schlögel et al., 2017). Visual tracking of recognizable man-made or slope features in multitemporal aerial and satellite-based images, as well as the identification and mapping of direct damages to infrastructures and buildings, can also provide clear evidence and quantification of

CONTACT Cecilia Fabbiani cecilia.fabbiani@unimore.it Department of Chemical and Geological Sciences, University of Modena and Reggio Emilia, Modena, Italy
Supplemental data for this article can be accessed online at https://doi.org/10.1080/17445647.2026.2693615.

ongoing gravitational deformations (Ma et al., 2021; Prokešová et al., 2010; Van Westen & Lulie Getahun, 2003).

This study deals with the Casale-Colla landslide in the Northern Apennines (Municipality of Ferriere, Piacenza Province, Italy) (Figure 1). The landslide

Figure 1. Geographic location and perspective view of the Casale-Colla landslide. Numbered points on the perspective view correspond to field photographs (shown below – all taken between January and March 2025) documenting significant damages to roads and buildings, as well as other ground evidence of the active landslide movements. Map showing the location of the Casale-Colla landslide in the Northern Apennines (Italy), with an inset 3D perspective view of the slope highlighting points of damage to roads and buildings.

extends over 0.42 km^2 from 1050 to 790 m a.s.l., and it is classified as a high-risk area by the Po River Basin Plan. The landslide causes damage to infrastructure, such as the national road SS654, and to nearby hamlets, including Colla di Gambaro, Casale, and Valle (Figure 2). No radiocarbon dating is available for the landslide, but its main features are already clearly recognizable in aerial images of 1976. By considering also that the damaged hamlets date back to the late nineteenth century, the origin of the landslide is to be referred to the Holocene.

The study area falls into the Geological Map of Italy at a 1:50,000 scale, Sheet 197 'Bobbio' (Elter et al., 1997). The outcropping formations belong to Sub-Ligurian Units, i.e. the Sanguineto and Canetolo Units. The upper portion of the slope is made up by the Salsominore Formation (FSN), consisting of massive, highly fractured calcareous rocks dipping into the slope (Figure 2). Locally, the FSN is dissected by a series of high-angle discontinuities, which have morphological evidence in ruptures along the main rock crest and in gullies. A lenticular body of the Canetolo Clays and Limestones (ACC) outcrops along the road SS654 and extends at the slope scale inside the FSN. Downslope, an overthrust separates the FSN from the Vico Flysch Formation (FVI), a calcareous-marly turbidite. The FVI, in turn, overthrusts the FSN unit toward the base of the slope.

2. Methods

In order to produce a detailed map and a set of representative geological cross-sections of the landslide, we have combined data regarding surface and subsurface features and movement rates. This section details the data collection, processing and integration procedures.

2.1. Archive data and multitemporal aerial orthoimages

The catalogue of landslide occurrences in the Emilia-Romagna Region (Piacentini et al., 2018) provides information on the Casale-Colla landslide (https://geo.regione.emilia-romagna.it/schede/fs/fs_dis.jsp?id=151484). It reports acceleration events and damages to the SS654 road and nearby villages in the years 1953, 1964, 1980, 1993, 1999, 2008 and 2014. Multitemporal aerial orthoimages are publicly available as web mapping services, dating back to 1976–78, 1994–98, 2006, 2018, 2020 (https://gn.mase.gov.it/portale/servizio-di-consultazione-wms; https://geoportale.regione.emilia-romagna.it/servizi/servizi-ogc/elenco-capabilities-dei-servizi-wms). All

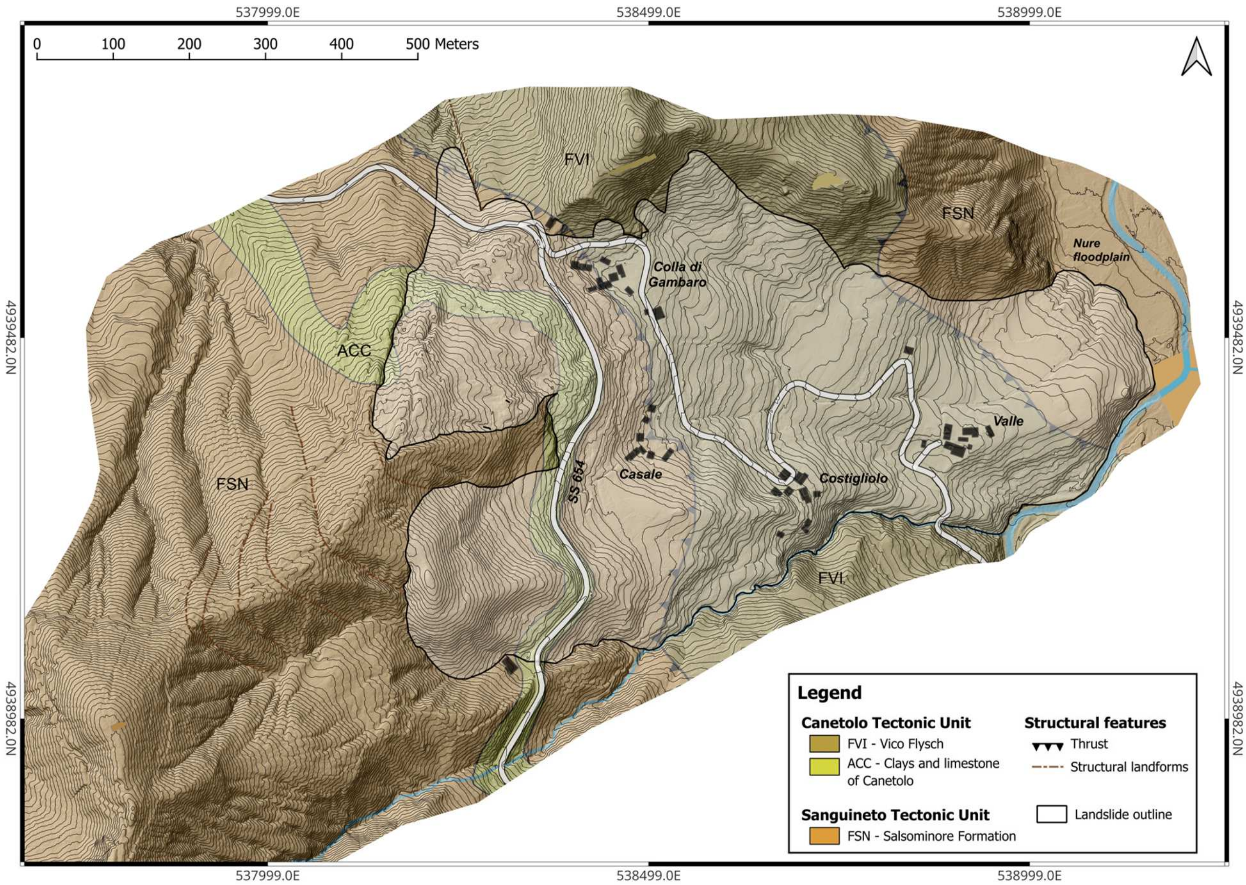

Figure 2. Geological overview of the study area (modified from the Geological Map of the Emilia-Romagna Region, 1:10,000 scale). Schematic geological map of the study area illustrating the Sanguineto and Canetolo Tectonic Units, the main rock formations (Salsominore, Canetolo Clays and Limestones, Vico Flysch), and major overthrust structures.

these orthoimages were visually analysed in GIS to identify landslide sectors that experienced significant evolution over time.

2.2. Surface displacement monitoring

2.2.1. Continuous GNSS monitoring

Since 2019, a continuous Global Navigation Satellite System (C-GNSS) monitoring system has been measuring surface displacements of the landslide. The system includes 3 Leica GMX901 receivers aligned from the upper to the lower part of the landslide (ROV3, ROV2 and ROV1) and 1 Leica GMX902 receiver in a stable position (master station). Displacement data are derived by differential correction of 1 h and 30 min RINEX data using Leica Spider software.

2.2.2. MT-InSAR analysis

For the years 2019-2025, a site-specific Multi-Temporal Interferometric SAR analysis (MT-InSAR) has been conducted by using Sentinel 1 satellite data. The analysis combined Persistent Scatterer Interferometry (PSI) and Distributed Scatterer Interferometry (DSI) in SARPROZ software (https://www.sarproz.com/). Both linear and non-parametric techniques were used to derive displacement time series. No atmospheric correction was used due to the limited extent of the analysed area. Two datasets with optimal point density and temporal coherence from PSI and DSI have been used for slope dynamics assessment. Both are from ascending orbit acquisitions, which ensure a better alignment between the satellite line of sight (LoS) and the expected slope movements direction (west to east).

2.3. Subsurface investigation and displacement monitoring

2.3.1. Borehole logging, inclinometers and piezometers

In 1999 and 2000, borehole investigation campaigns, with the installation of inclinometers and piezometers, were conducted by the Regional Office of Civil Engineering. We have collected the core-logging reports compiled at the time, as well as the inclinometer plots and data tables. The 1999 campaign included 6 continuous coring (c.c.) equipped with inclinometer tubes (I1–I7) and 6 core destruction (c.d.) boreholes equipped with open-pipe piezometers (P1–P7). An additional c.c. borehole (D3) was left unequipped. Reference measurements date from 4th to 7th November 2019, followed by monitoring from 1st to 18th November 1999. The 2000 campaign included 3 c.d. boreholes with new inclinometer casings (I2 bis, I4 bis, I5 bis), replacing those previously sheared by landslide movement. Reference measurements date from 22nd March 2000, and monitoring continued until 9th October 2000. Piezometric levels were measured using an electric tape during inclinometer readings. Although the number of boreholes and instruments installed was limited and several inclinometers were quickly damaged by movement, these data provided valuable insights into the lithological characteristics of the landslide materials, the depth of basal and secondary shear surfaces, and the position of the groundwater table.

2.3.2. P-waves seismic refraction

In the year 2000, a campaign of P-wave seismic refraction surveys was conducted by the Regional Office of Civil Engineering. Data were acquired along multiple seismic spreads using a 12-channel seismograph and 14 Hz vertical geophones. Each spread measured 110–116 m, with 10 m geophone spacing, and received multiple energizations. Data processing was performed using the intercept and delay-time (Gardner) methods, resulting in P-wave velocity profiles. For this study, we have collected and analysed the P-wave velocity profiles located along or near the selected reference cross-sections. Such data have supported the identification of the contact between different landslide sub-units, and between landslide deposits and bedrock.

2.4. UAV-Lidar and field surveys

In March 2024, we have carried out a LiDAR and trichromatic (RGB) survey of the landslide area, by using an Unmanned Aerial Vehicle (UAV). Specifically, we have used a DJI Matrice 350 RTK equipped with a penta-returns DJI Zenmuse L2 LiDAR sensor (DJI Technology Co., Ltd., Shenzhen, China). The survey has resulted in a 25 cm pixel Digital Terrain Model (DTM) and a 5 cm pixel RGB-colouring orthoimages of the landslide area and surrounding slopes. Hillshades derived from the DTM and the orthoimage have been used as basis for mapping landslide features, for the identification of landslide sub-units, and for the extraction of updated topographic profiles for the representative cross-sections. Field surveys conducted in 2024 and 2025 have allowed to refine geomorphological mapping, to document several pieces of surface evidence of slope movements and to analyse bedrock outcrops in terms of lithology and dip direction and angle of strata.

2.5. Landslide mapping and cross-sections layout

Following the approach proposed by Pasuto and Soldati (1999), we have defined the Casale-Colla 'landslide unit' as an ensemble of several morpho-kinematic 'landslide sub-units', which are distinct on the basis of morphological features, movement rate and materials involved. These sub-units represent landslide deposits strictly connected to the progressive evolution of the landslide in space and time and derive from a juxtaposition and superposition of rupture, depletion and accumulation events. The identification of sub-units has been based on geomorphological evidence (collected in field surveys and by interpretation of the hillshades and contour lines derived from the Lidar DEM), multitemporal aerial photos interpretation, as well as on C-GNSS and MT-InSAR monitoring, which show variable displacement rates and directions. Each sub-unit has been further subdivided into landslide elements, in order to account for second order morphological features. In the main map, sub-units have been represented by using different background colours, so as to provide an 'at a glance' vision of their distribution, with overimposed black symbols representing the type of movement. Furthermore, the main map includes line symbols tracing the edge of the main and secondary landslide scarps, as well as structural discontinuities that are believed to have controlled the landslide evolution. In the reference cross-sections, data from mapping, inclinometers, borehole stratigraphy and refraction seismic have been combined to exemplify the reciprocal spatial and kinematical relationships among sub-units. Cross-sections show the transition from roto-translational to translational movements, the materials involved and the depths of multiple sliding surfaces.

3. Results

3.1. Multitemporal orthoimages analysis

The analysis of multitemporal orthoimages indicates a significant landslide evolution in the last 50 years. This is particularly evident in two areas: the head part of the landslide, and the section of the landslide which stretches from SS654 to the Colla di Gambaro hamlet (Figure 3). In the head part of the landslide, fractures affecting the limestones have significantly widened and deepened, evidencing a block-like displacement in the SW-NE direction. Tracking of fractures indicates an approximate 16 m planimetric displacement from 1976–1978 to 2024, corresponding to an average rate of about 0.33-0.35 m/y. At the same time, the SS 654 road has been shifted toward east for about 14.5 m. In the hamlet of Colla di Gambaro, some buildings can be tracked for over a 10 m planimetric displacement in the same period. It should be noted that the stability over time of a building located outside the northern boundary of the landslide provides evidence that the observed displacements within the landslide are not due to georeferencing artefacts.

3.2. Surface displacements

The C-GNSS monitoring for the 2020–2025 period indicates displacements of about 3.2 m at ROV3 (average 0.59 m/y), 1.6 m at ROV2 (average 0.30 m/y) and 0.7 m at ROV1 (average 0.12 m/y) (Figure 4 and Figure 5a). Displacement direction varies along the slope (to NE for ROV3, to E for ROV2 and ROV1; see markers orientation in Figure 4). A comparison of displacement time series and cumulated rainfall recorded at the Selva-Ferriere gauge station (located 4 km south of the landslide; altitude: 1109 m asl; Coord (Lat, Long): 44.586768, 9.482447) reveals accelerations in response to prolonged cumulated rainfall (Figure 5). Altogether, data show that displacement rates are significantly higher in the upper-intermediate part of the landslide than in the lower part. They also show that velocity variations during the years are modulated by monthly cumulated rainfall.

The MT-InSAR displacement data along the LoS are qualitatively consistent with C-GNSS data, but underestimate movement rates by one order of magnitude (Figure 3 and Figure 5b). For instance, near the hamlets of Colla di Gambaro and Casale, LoS velocity is in the range 30–60 mm/y (while the nearby ROV2 moves at 0.30 m/y). At the same time, LoS velocity is in the range of 10–30 mm/y near the hamlet of Valle in the lower part of the landslide. At the village of Costigliolo, LoS velocity is less than 5 mm/y, as it is in the southernmost part of the landslide. Near Costigliolo, some local active deformation is evidenced by points in the range of 5–10 mm/y, which are also causing some fractures on the local road.

3.3. Subsurface landslide stratigraphy and depth of movements

Inclinometers installed in 1999 and 2000 have detected multiple shear surfaces and have rapidly been sheared by movements (see Figure 6 for location and Table 1 for data). In the northern and upper sectors of the landslide, the depth of the basal sliding surface has been detected at maximum 38 m, while secondary sliding surfaces, cutting inside the landslide mass, have been found at depths of 16–20 m (see data from I7, I1, I2, I2bis). At the same time, in the northern and lower sectors of the landslide, the depth of the basal sliding surface has been measured at a maximum of 33 m, with secondary surfaces at 17 m depth (see data from I5, I5bis, I6). In contrast, near Casale (in the southern sector of the landslide), the depth of sliding surfaces is limited to 7 m (see data from inclinometers I4, I4bis). Borehole logs indicate that the basal sliding surface corresponds to the contact between the landslide body (made of highly fractured limestones, or of blocks in matrix deposits) and the bedrock. Refraction seismic profiles indicate a

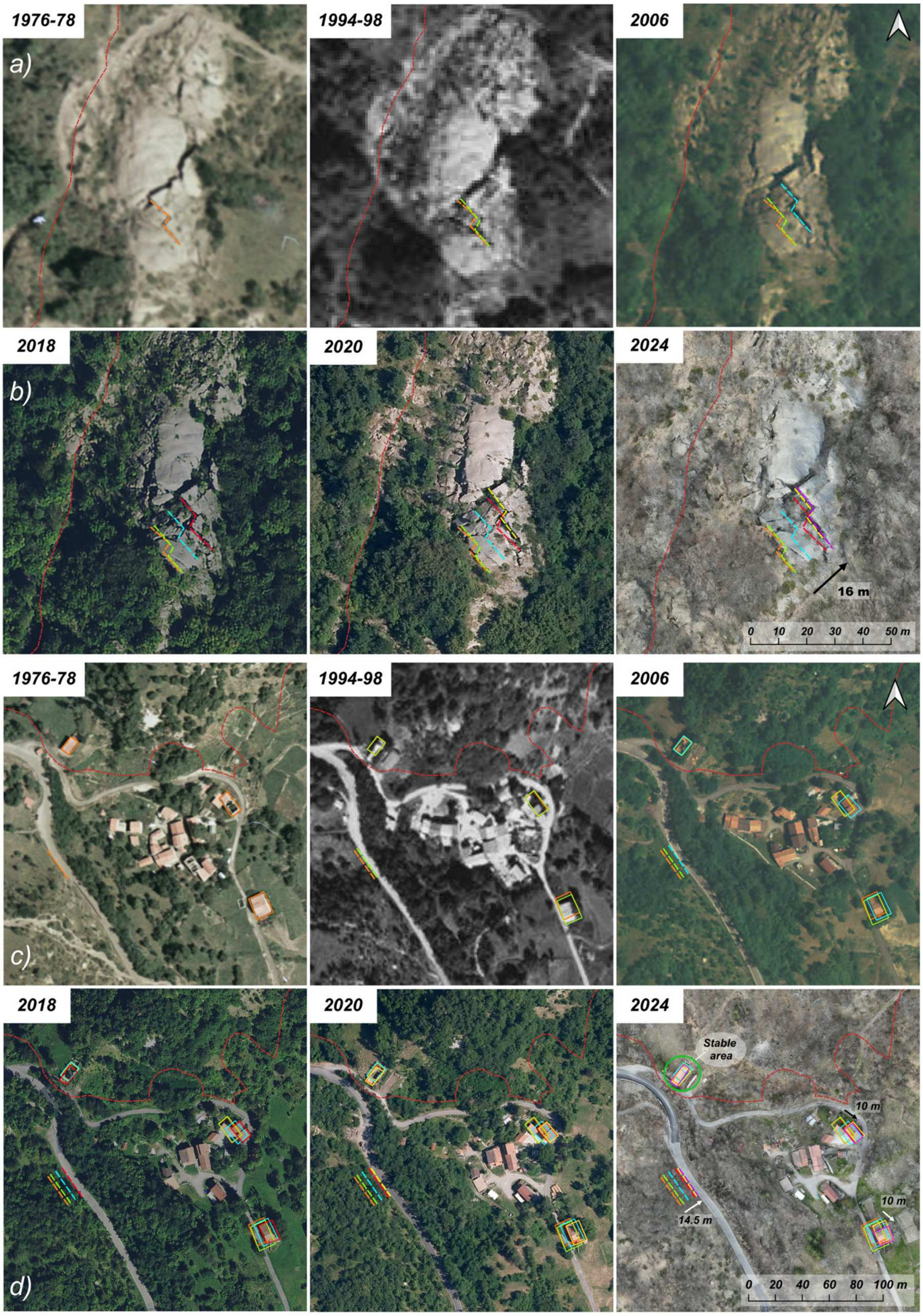

Figure 3. Comparisons of multitemporal orthoimages from 1976–1978 to 2024 from two selected sectors within the landslide: highly fractured rock outcrop (a-b) and the buildings and infrastructure near and in the village of Colla di Gambaro (c-d). Photo locations are shown in Figure 6. Side-by-side comparison of aerial orthophotos from 1976–1978 and 2024, showing the widening of fractures in the landslide head scarp and the eastward displacement of buildings and a road in the Colla di Gambaro hamlet.

significant increase in P-wave velocity at depths roughly corresponding to the basal sliding surfaces. Available piezometric data, although limited in temporal and spatial coverage, suggest that groundwater levels are broadly consistent with the depth of the identified sliding surfaces. This provides

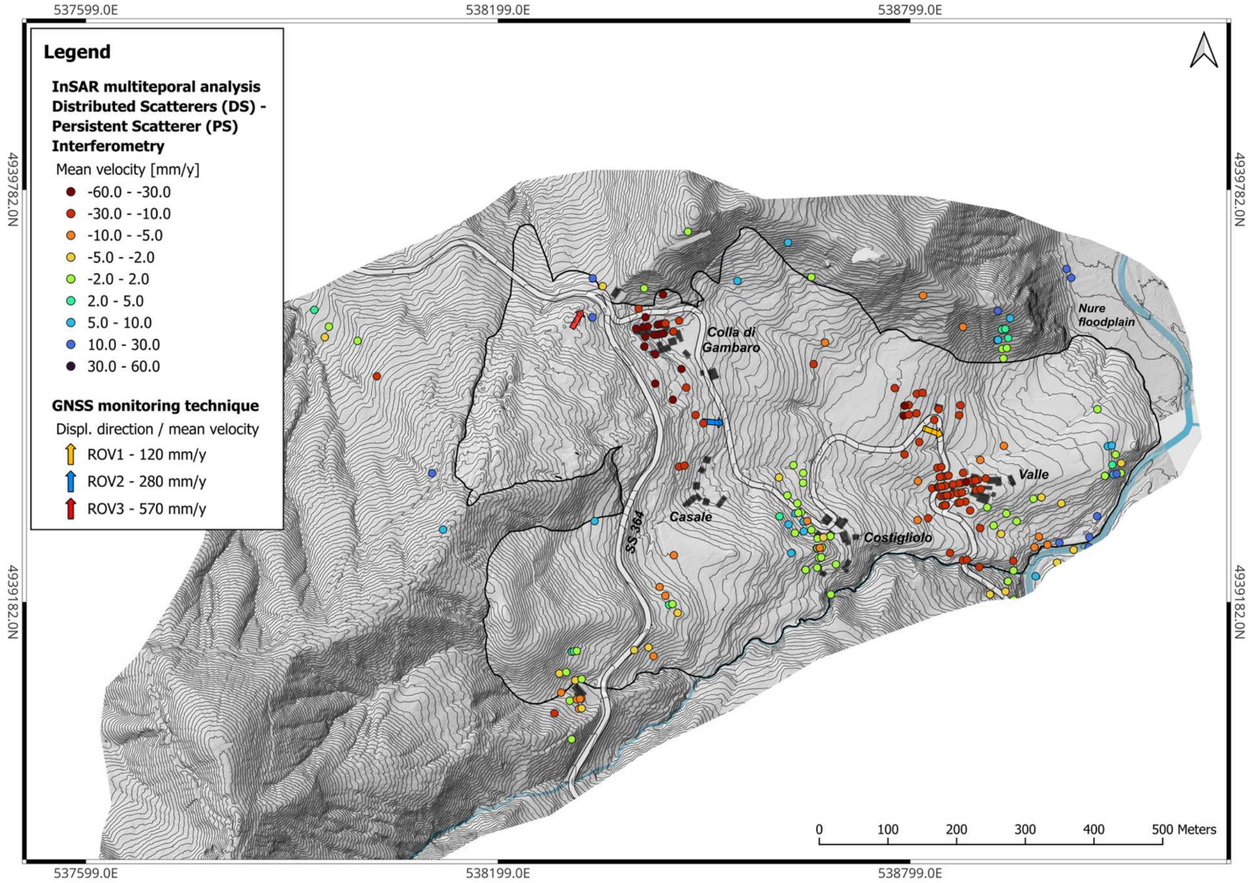

Figure 4. Integration of MT-InSAR (Sentinel-1, ascending orbit) and C-GNSS monitoring data. GNSS rover stations (ROV1-3) show both direction of displacement (arrows) and mean velocity. The selected MT-InSAR data (PSI and DSI) represent the spatial distribution of mean velocity rates across the landslide body. Map of the landslide body coloured by mean velocity from MT-InSAR data, overlaid with arrows from C-GNSS stations (ROV1, ROV2, ROV3) showing displacement direction and magnitude.

qualitative support for the interpretation that groundwater plays a key role in controlling landslide dynamics.

3.4. Landside map and reference cross sections

The Casale-Colla landslide map (Main Map) provides a comprehensive geological model for interpreting the complexity of the phenomenon. The map shows that the landslide can be subdivided into 5 main sub-units, whose morphometric and kinematic characteristics are summarized in Table 2. In the northern sector, sub-units A, B and C reflect a progressive transition from an active deep-seated rotational rock slide in the upper sector, to an active translational earth slide downslope. In these sub-units, surface and subsurface monitoring data indicate a decreasing displacement rate from the A to the C sub-units. This is consistent with the widespread presence of field evidences of active slope deformations in sub-units A and B, such as road fractures, depressions, bulges, and structural damage to buildings, and with a more limited presence of such evidence in sub-unit C. In the southern sector, sub-unit D is a deep-seated roto-translational rock slide, that can be considered substantially dormant, as MT-InSAR data indicate a generalized absence of active movements, except for the presence of some localized deformations in limited areas. In the northern and southern sectors, sub-unit E has been introduced to group several localized secondary earth slides, which are superimposed on the main landslide body. For sub-units D and E, where direct information on sliding surface depth is not available, volumes were estimated based on morphometric considerations. In particular, depth was qualitatively inferred from the geometry of the sub-units (length, width, and geomorphological expression) and by analogy with the better-constrained sub-units A, B and C; therefore, these values should be regarded as first-order approximations (Table 2). The representative cross-sections of the most active part of the landslide, which includes sub-units A, B and C, evidence that the geometry and initiation of failure surfaces in sub-unit A are structurally controlled by pre-existing discontinuities within the FSN bedrock formation, confirming the fundamental influence of geological setting on slope instability. The cross-sections also indicate the most likely geometry of the overthrusts separating FSN and FVI bedrock formations, which exerts a structural and hydrogeological control on the basal sliding surfaces of the landslide. The cross-sections provide an interpretative framework for the transition

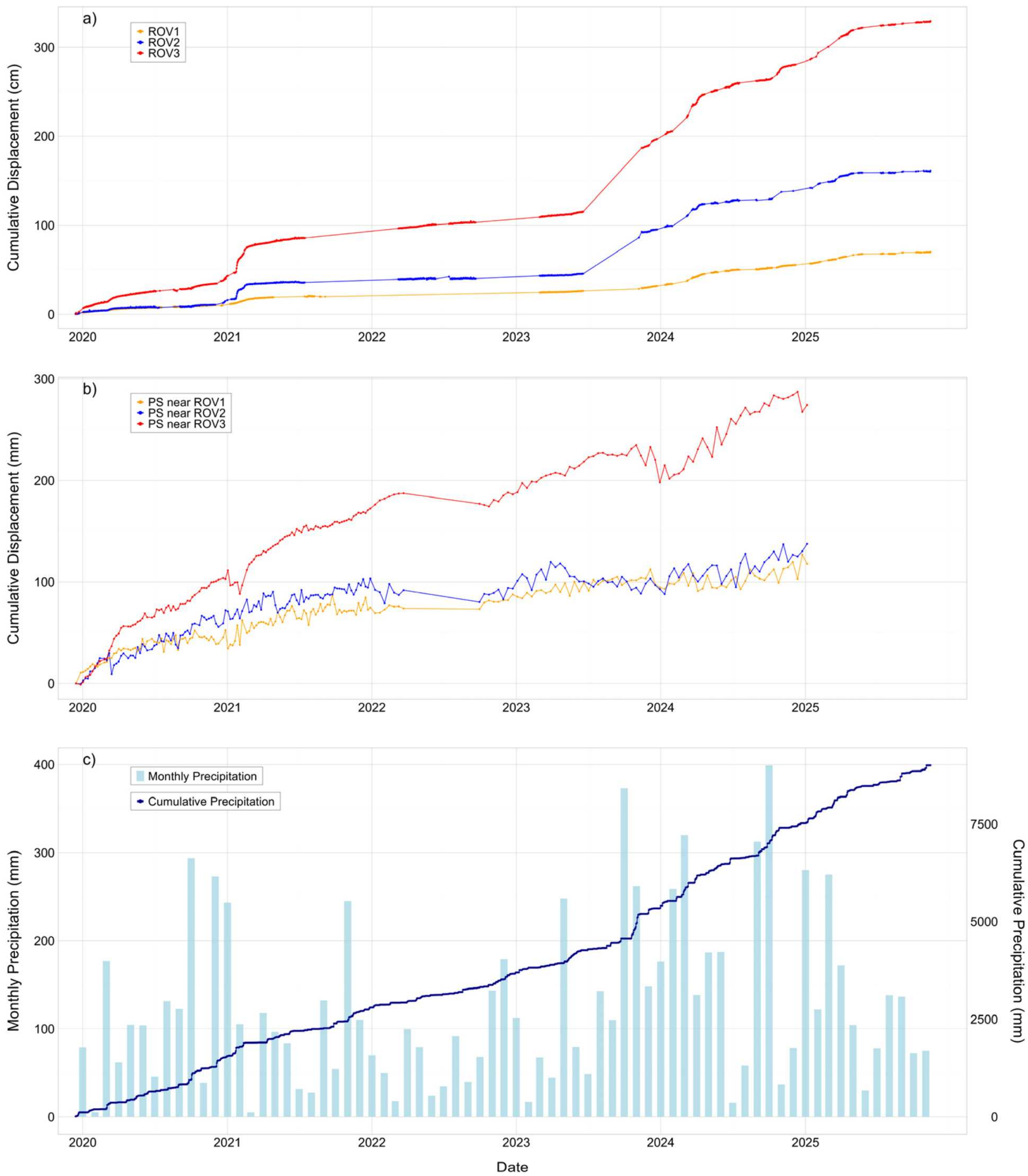

Figure 5. (#a) Cumulative planimetric displacement recorded by the continuous GNSS stations (ROV1, 2, 3) from 2020 to 2025. The plot shows displacement rates decreasing from the upper to the intermediate and lower part of the landslide (ROV3, ROV2 and ROV1, respectively). (b) InSAR displacement time-series from 2019 to 2025, for selected PS and DS located near to the C-GNSS rovers. The plot shows that InSAR time-series are qualitatively consistent with C-GNSS data (see Figure 4), but the calculated displacement rates are underestimated by one order of magnitude. (Note: the original ascending orbit data, where negative values indicate movement away from the satellite, have been sign-inverted to facilitate direct comparison with the C-GNSS dataset). (c) Monthly and cumulative rainfall recorded at the Selva Ferriere rain gauge during the same monitoring period, showing a direct correlation between periods of significant cumulated precipitation and acceleration of landslide movement. Three time-series graphs. Graph (a) shows cumulative GNSS displacement, with rates decreasing downslope. Graph (b) compares C-GNSS and MT-InSAR displacement, showing qualitative agreement but magnitude underestimation. Graph (c) plots monthly and cumulative rainfall, demonstrating how movement accelerations correlate with peaks in precipitation.

from rock sliding to earth sliding from sub-unit A to B and C. In such framework, the decreasing movement rates along the slope are justified by assuming that sub-unit A overthrusts sub-unit B, which in turn overthrusts sub-unit C. Such a stacked geometry explains why displacement rates in sub-unit A are roughly twice those in sub-unit B, and a similar ratio occurs between sub-units B and C. The depths of

Table 1. Summary of inclinometer readings (RM = Reference Measurements; S1 deepest slide surface; S2 shallower slide surface)

Inclinometer	Length	04/11/1999	05/11/1999	07/11/1999	11/11/1999	18/11/1999	20/03/2000	09/10/2000
I7	70 m		RM	S1: 29 m	S1: 29 m	Sheared at 29 m		
I1	90 m		RM	S2: 16 m S1 33 m	S2: 16 m S1 33 m	Sheared at 33 m		
I2	60 m			RM	S2: 20 m S1 38 m	Sheared at 38 m		
I2bis	25 m						RM	S1: 21 m
I4	35 m	RM	S2: 4 m S1 7 m	S2: 4 m S1 7 m	S2: 4 m S1 7 m	Sheared at 7 m		
I4bis	10.5 m						RM	S1: 7 m
I5	35 m	RM	S2: 17 m S1: 33 m	S2: 17 m S1: 33 m	S2: 17 m S1: 33 m	Sheared at 17 m		
I5 bis	20 m						RM	S1: 17 m
I6	40 m	RM	S1 17 m S1: 31 m	S1 17 m S1: 31 m	S1 17 m S1: 31 m	S1 17 m S1: 31 m	S1 17 m S1: 31 m	S1 17 m S1: 31 m

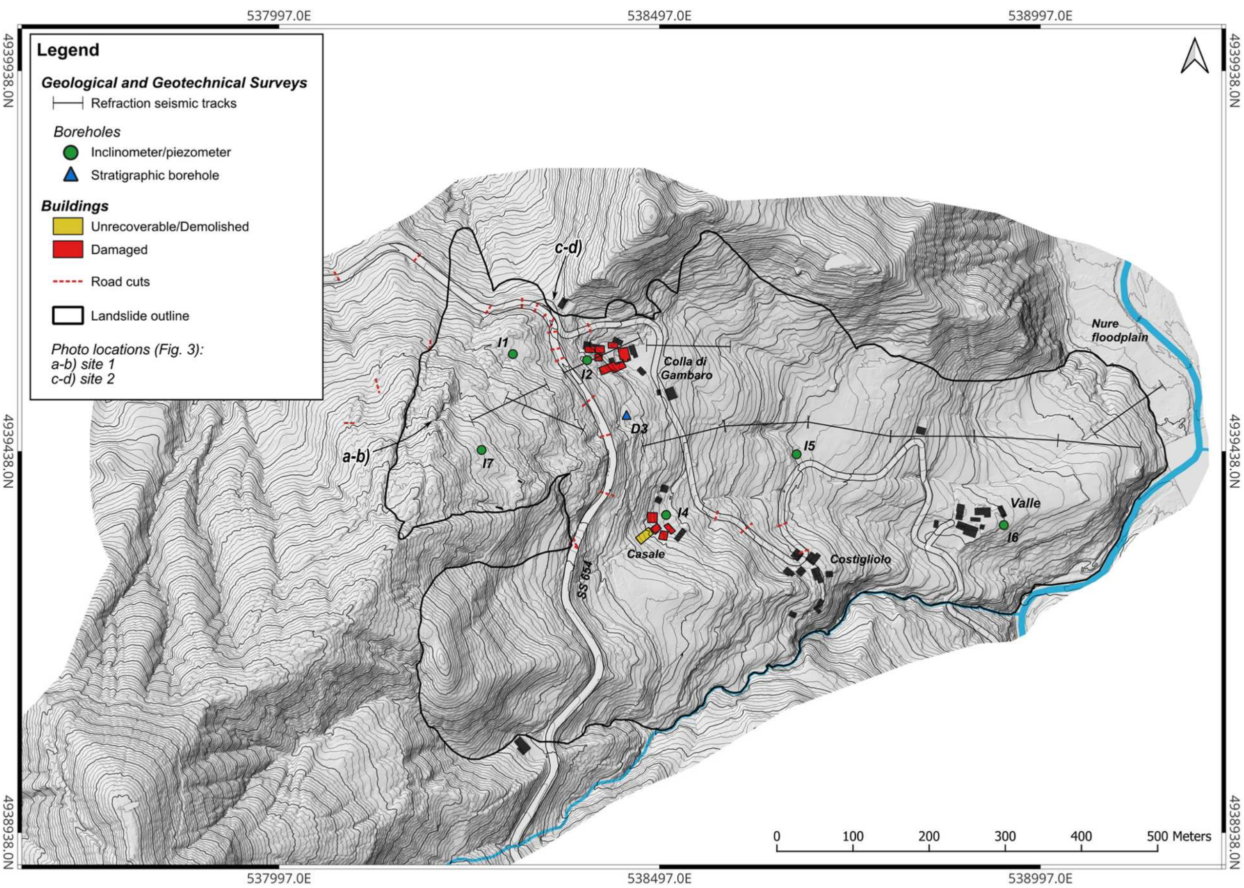

Figure 6. Map showing the location of existing datasets integrated into the study: seismic refraction tracks used for cross-section profiling, boreholes (inclinometer/piezometer-equipped), field-verified road cuts and buildings, and the delineated landslide boundary. Photo locations corresponding to Figure 3 (a–d) are also indicated. Map of the landslide indicating the locations of integrated datasets, including boreholes with inclinometers/piezometers, seismic refraction survey lines, damaged buildings used for ground-truthing, and the locations of the photographs shown in Figure 3.

Table 2. Morphometric and kinematic characteristics of the Casale-Colla landslide sub-units (ND = undetermined).

SUB-UNIT	A	B	C	D	E
Kinematics	Rotational slide	Translational slide	Translational slide	Roto-trasl. slide	Translational slide
Material	Rock (FSN)	Earth	Earth	Rock (FSN)	Earth
Area (m^2)	100,430	68,400	106,720	119,400	22,950
Length (m)	400	300	500	790	190
Width (m)	480	350	310	250	100
L/W ratio	0.83	0.86	1.61	3.16	1.90
Slope (°)	21	17	14	22	20
Max depth (m)	40	37.5	30	ND	ND
Volume (m^3)	4,017,240	2,564,870	3,201,380	4,180,550	515,840

shear surfaces evidenced by inclinometers are compatible with such interpretation, as they allow for locating sub-unit contacts at depth and for recognize basal and secondary sliding surfaces, at a maximum depth of about 40 m. Monitoring data indicate a correlation between displacement rates and monthly rainfall patterns, suggesting that groundwater acts as the primary controlling mechanism, as also qualitatively supported by available piezometric data. This will require further specific analyses and, possibly, modelling. For the aim of which, the produced cross-sections will constitute a reference geological model.

4. Conclusions

Landslide mapping is the basis for hazard and risk zoning, as well as for the identification of possible consolidation works or early warning rules (Corominas et al., 2013; Guzzetti et al., 1999, 2006; Roccati et al., 2021; Spinetti et al., 2019; 2003). The case study of the Casale-Colla landslide, zoned as a high-risk area by the Po River Basin Plan, demonstrates that landslide mapping and the understanding of driving mechanisms can be significantly improved by the integration of traditional and innovative monitoring investigations and monitoring techniques. In perspective, the map and the cross-sections produced offer a reliable geological framework to improve the consistency and detail of landslide risk zonation for the Casale-Colla landslide and to prioritize possible stabilization works for the protection of critical infrastructure, including the SS654 road. Furthermore, the correlation between rainfall and movement rates revealed by this study opens up the opportunity to develop rainfall-based early-warning thresholds. The methodology adopted is replicable in other large-scale landslides that show complex and composite characteristics and that require a similar level of detailed analysis.

Software

All geospatial data and the detailed map were processed in QGIS Desktop 3.40.5. Cross-sections were generated from QGIS topographic profiles, drafted in AutoCAD 2025, and finalized in Inkscape, which was also used for the A0 main map layout.

Acknowledgements

This study is part of the activities of the project ‘Study, monitoring and modelling of large landslides affecting the province of Piacenza’, financed by the Emilia-Romagna Region, Agency for Territorial Security and Civil Protection – Office of Piacenza (D.G.R. 450/22 L.R. 7/2004 COD SE22A003)

Author contributions

CRediT: **Cecilia Fabbiani:** Conceptualization, Data curation, Formal analysis, Investigation, Methodology, Resources, Software, Writing – original draft; **Marco Mulas:** Conceptualization, Data curation, Methodology, Project administration, Supervision, Writing – review & editing; **Vincenzo Critelli:** Data curation, Investigation, Resources; **Irene Ghiselli:** Investigation, Resources; **Jean Pascal Iannacone:** Data curation, Investigation, Resources; **Francesco Lelli:** Data curation, Investigation, Resources; **Melissa Tondo:** Data curation, Investigation, Resources; **Giovanni Truffelli:** Investigation, Resources; **Alessandro Corsini:** Conceptualization, Funding acquisition, Methodology, Project administration, Supervision, Visualization, Writing – review & editing.

Disclosure statement

No potential conflict of interest was reported by the author(s).

Funding

This work was supported by the University of Modena and Reggio Emilia – PhD Grant – Course in “Models and Methods for Material and Environmental Sciences”.

Data availability statement

The data that support the findings of this study are available from the corresponding author upon reasonable request. Requests for data will be assessed on a case-by-case basis to ensure compliance with ethical, privacy, and security considerations.

References

Agliardi, F., Crosta, G., & Zanchi, A. (2001). Structural constraints on deep-seated slope deformation kinematics. *Engineering Geology*, *59*, 83–102. https://doi.org/10.1016/S0013-7952(00)00066-1

Bozzano, F., Carabella, C., De Pari, P., Discenza, M. E., Fantucci, R., Mazzanti, P., Miccadei, E., Rocca, A., Romano, S., & Sciarra, N. (2020). Geological and geomorphological analysis of a complex landslides system: The case of San Martino sulla Marruccina (Abruzzo, Central Italy). *Journal of Maps*, *16*(2), 126–136. https://doi.org/10.1080/17445647.2019.1702596

Bozzano, F., Mazzanti, P., Perissin, D., Rocca, A., De Pari, P., & Discenza, M. E. (2017). Basin scale assessment of landslides geomorphological setting by advanced InSAR analysis. *Remote Sensing*, *9*(3), 267–219. https://doi.org/10.3390/rs9030267

Bucci, F., Santangelo, M., Fiorucci, F., Ardizzone, F., Giordan, D., Cignetti, M., Notti, D., Allasia, P., Godone, D., Lagomarsino, D., Pozzoli, A., Norelli, E., & Cardinali, M. (2021). Geomorphologic landslide inventory by air photo interpretation of the high agri valley (Southern Italy). *Journal of Maps*, *17*(2), 376–388. https://doi.org/10.1080/17445647.2021.1943552

Bufalini, M., Materazzi, M., De Amicis, M., & Pambianchi, G. (2021). From traditional to modern ‘full coverage’ geomorphological mapping: A study case in the Chienti River basin (Marche region, central Italy). *Journal of*

Maps, *17*(3), 17–28. https://doi.org/10.1080/17445647.2021.1904020
Carrara, A., Crosta, G., & Frattini, P. (2003). Geomorphological and historical data in assessing landslide hazard. *Earth Surface Processes and Landforms*, *28*(10), 1125–1142. https://doi.org/10.1002/esp.545
Cenni, N., Fiaschi, S., & Fabris, M. (2021). Integrated use of archival aerial photogrammetry, GNSS, and InSAR data for the monitoring of the Patigno landslide (Northern Apennines, Italy). *Landslides*, *18*(6), 2247–2263. https://doi.org/10.1007/s10346-021-01635-3
Chelli, A., Bordoni, M., Cappadonia, C., Pepe, G., Rotigliano, E., & Smith, M. (2021). Geomorphological tools for mapping natural hazards. *Journal of Maps*, *17*(3), 1–4. https://doi.org/10.1080/17445647.2021.1920794
Chelli, A., Segadelli, S., Vescovi, P., & Tellini, C. (2016). Large-scale geomorphological mapping as a tool to detect structural features: the case of Mt. Prinzera ophiolite rock mass (Northern Apennines, Italy). *Journal of Maps*, *12*(5), 770–776. https://doi.org/10.1080/17445647.2015.1072115
Ciccarese, G., Tondo, M., Mulas, M., Bertolini, G., & Corsini, A. (2024). Rapid assessment of landslide dynamics by UAV-RTK repeated surveys using ground targets: The Ca' Lita landslide (northern Apennines, Italy). *Remote Sensing*, *16*(6), 1032. https://doi.org/10.3390/rs16061032
Ciuffi, P., Bayer, B., Berti, M., Franceschini, S., & Simoni, A. (2024). InSAR stacking to detect active landslides and investigate their relation to rainfalls in the northern Apennines of Italy. *Geomorphology*, *457*, 109242–15. https://doi.org/10.1016/j.geomorph.2024.109242
Corominas, J., van Westen, C., Frattini, P., Cascini, L., Malet, J. P., Fotopoulou, S., Catani, F., Van Den Eeckhaut, M., Mavrouli, O., Agliardi, F., Pitilakis, K., Winter, M. G., Pastor, M., Ferlisi, S., Tofani, V., Hervás, J., & Smith, J. T. (2013). Recommendations for the quantitative analysis of landslide risk. *Bulletin of Engineering Geology and the Environment*, *73*(2), 209–263. https://doi.org/10.1007/s10064-013-0538-8
Corsini, A., Bonacini, F., Mulas, M., Petitta, M., Ronchetti, F., & Truffelli, G. (2015). Long-Term continuous monitoring of a deep-seated compound rock slide in the northern Apennines (Italy). In G. Lollino, D. Giordan, G. B. Crosta, J. Corominas, R. Azzam, J. Wasowski, & N. Sciarra (Eds.), *Engineering geology for society and territory* (Vol. 2, pp. 1337–1340). Springer International Publishing.
Devoto, S., Macovaz, V., Mantovani, M., Soldati, M., & Furlani, S. (2020). Advantages of using UAV digital photogrammetry in the study of slow-moving coastal landslides. *Remote Sensing*, *12*(21), 3566–3527. https://doi.org/10.3390/rs12213566
Dotta, G., Fornaciai, A., Bertolini, G., Isola, I., Nannipieri, L., Favalli, M., Burrato, P., Devoti, R., Gigli, G., Mucchi, L., Intrieri, E., Pizziolo, M., Gracchi, T., & Casagli, N. (2023). Geomorphology of the upper sector of the Roncovetro active landslide (Emilia-Romagna Region, Italy). *Journal of Maps*, *19*(1), 1–11. https://doi.org/10.1080/17445647.2023.2277898
Elter, P., Ghiselli, F., Marroni, M., & Ottria, G. (1997). *Note illustrative della carta geologica d'Italia in scala 1:50.000 - Foglio 197, 'Bobbio'*. Istituto Poligrafico e Zecca dello Stato.
Fioraso, G. (2017). Impact of massive deep-seated rock slope failures on mountain valley morphology in the northern cottian Alps (Nw Italy). *Journal of Maps*, *13*(2), 575–587. https://doi.org/10.1080/17445647.2017.1342211
Giacomelli, S., Leonelli, G., Gemignani, C. A., & Chelli, A. (2021). Geo-historical study for landslide hazard assessment in territory management: The casaleto-illica landslide in the ceno valley (northern Apennines, Italy). *Journal of Maps*, *17*(3), 100–110. https://doi.org/10.1080/17445647.2021.1908186
Guzzetti, F., Carrara, A., Cardinali, M., & Reichenbach, P. (1999). Landslide hazard evaluation: A review of current techniques and their application in a multi-scale study, central Italy. *Geomorphology*, *31*, 181–216. https://doi.org/10.1016/S0169-555X(99)00078-1
Guzzetti, F., Mondini, A. C., Cardinali, M., Fiorucci, F., Santangelo, M., & Chang, K. T. (2012). Landslide inventory maps: New tools for an old problem. *Earth-Science Reviews*, *112*(1–2), 42–66. https://doi.org/10.1016/j.earscirev.2012.02.001
Guzzetti, F., Reichenbach, P., Ardizzone, F., Cardinali, M., & Galli, M. (2006). Estimating the quality of landslide susceptibility models. *Geomorphology*, *81*(1–2), 166–184. https://doi.org/10.1016/j.geomorph.2006.04.007
Jaboyedoff, M., Oppikofer, T., Abellán, A., Derron, M. H., Loye, A., Metzger, R., & Pedrazzini, A. (2012). Use of LIDAR in landslide investigations: A review. *Natural Hazards*, *61*(1), 5–28. https://doi.org/10.1007/s11069-010-9634-2
Johnson, S. E., Haneberg, W. C., Bryson, L. S., & Crawford, M. M. (2023). Measuring ground surface elevation changes in a slow-moving colluvial landslide using combinations of regional airborne lidar, UAV lidar and UAV photogrammetric surveys. *Quarterly Journal of Engineering Geology and Hydrogeology*, *56*(2), qjegh2022-078. https://doi.org/10.1144/qjegh2022-078
Lee, E. M. (2001). Geomorphological mapping. *Geological Society Special Publication*, *18*(1), 53–56. https://doi.org/10.1144/gsl.eng.2001.018.01.08
Lelli, F., Mulas, M., Critelli, V., Fabbiani, C., Tondo, M., Aleotti, M., & Corsini, A. (2025). Leveraging high-frequency UAV–LiDAR surveys to monitor earthflow dynamics—The Baldiola landslide case study. *Remote Sensing*, *17*(15), 2657. https://doi.org/10.3390/rs17152657
Ma, S., Qiu, H., Hu, S., Yang, D., & Liu, Z. (2021). Characteristics and geomorphology change detection analysis of the Jiangdingya landslide on July 12, 2018, China. *Landslides*, *18*(1), 383–396. https://doi.org/10.1007/s10346-020-01530-3
Mantovani, M., Bossi, G., Dykes, A. P., Pasuto, A., Soldati, M., & Devoto, S. (2022). Coupling long-term GNSS monitoring and numerical modelling of lateral spreading for hazard assessment purposes. *Engineering Geology*, *296*, 106466, https://doi.org/10.1016/j.enggeo.2021.106466
Mondini, A. C., Guzzetti, F., Chang, K. T., Monserrat, O., Martha, T. R., & Manconi, A. (2021). Landslide failures detection and mapping using synthetic aperture radar: Past, present and future. *Earth-Science Reviews*, *216*, 103574–33. https://doi.org/10.1016/j.earscirev.2021.103574
Mulas, M., Ciccarese, G., Truffelli, G., & Corsini, A. (2020a). Displacements of an active moderately rapid landslide—A dataset retrieved by continuous gnss arrays. *Data*, *5*(3), 71–76. https://doi.org/10.3390/data5030071
Mulas, M., Ciccarese, G., Truffelli, G., & Corsini, A. (2020b). Integration of digital image correlation of sentinel-2 data and continuous gnss for long-term slope movements monitoring in moderately rapid landslides. *Remote*

Sensing, *12*(16), 2605–2617. https://doi.org/10.3390/RS12162605

Pasuto, A., & Soldati, M. (1999). The use of landslide units in geomorphological mapping: An example in the Italian dolomites. *Geomorphology*, *30*, 53–64. https://doi.org/10.1016/S0169-555X(99)00044-6

Pawluszek, K. (2019). Landslide features identification and morphology investigation using high-resolution DEM derivatives. *Natural Hazards*, *96*(1), 311–330. https://doi.org/10.1007/s11069-018-3543-1

Pellicani, R., Argentiero, I., Manzari, P., Spilotro, G., Marzo, C., Ermini, R., & Apollonio, C. (2019). UAV and airborne LiDAR data for interpreting kinematic evolution of landslide movements: The case study of the Montescaglioso landslide (southern Italy). *Geosciences*, *9*(1), 6248. https://doi.org/10.3390/geosciences9060248

Piacentini, D., Troiani, F., Daniele, G., & Pizziolo, M. (2018). Historical geospatial database for landslide analysis: The catalogue of landslide occurrences in the Emilia-Romagna region (CLOCkER). *Landslides*, *15*(4), 811–822. https://doi.org/10.1007/s10346-018-0962-8

Prokešová, R., Kardoš, M., & Medveďová, A. (2010). Landslide dynamics from high-resolution aerial photographs: A case study from the western Carpathians, Slovakia. *Geomorphology*, *115*(1–2), 90–101. https://doi.org/10.1016/j.geomorph.2009.09.033

Roccati, A., Paliaga, G., Luino, F., Faccini, F., & Turconi, L. (2021). Gis-based landslide susceptibility mapping for land use planning and risk assessment. *Land*, *10*(2), 162–128. https://doi.org/10.3390/land10020162

Santangelo, M., Marchesini, I., Bucci, F., Cardinali, M., Cavalli, M., Crema, S., Marchi, L., Alvioli, M., & Guzzetti, F. (2021). Exposure to landslides in rural areas in central Italy. *Journal of Maps*, *17*(4), 124–132. https://doi.org/10.1080/17445647.2020.1746699

Scaioni, M., Longoni, L., Melillo, V., & Papini, M. (2014). Remote sensing for landslide investigations: An overview of recent achievements and perspectives. *Remote Sensing*, *6*, 1–53. https://doi.org/10.3390/rs6109600

Schlögel, R., Thiebes, B., Mulas, M., Cuozzo, G., Notarnicola, C., Schneiderbauer, S., Crespi, M., Mazzoni, A., Mair, V., & Corsini, A. (2017). Multi-temporal x-band radar interferometry using corner reflectors: Application and validation at the Corvara landslide (Dolomites, Italy). *Remote Sensing*, *9*(7), 739–720. https://doi.org/10.3390/rs9070739

Spinetti, C., Bisson, M., Tolomei, C., Colini, L., Galvani, A., Moro, M., Saroli, M., & Sepe, V. (2019). Landslide susceptibility mapping by remote sensing and geomorphological data: Case studies on the Sorrentina Peninsula (southern Italy). *GIScience & Remote Sensing*, *56*(6), 940–965. https://doi.org/10.1080/15481603.2019.1587891

Sterzai, P., Vellico, M., Berti, M., Coren, F., Corsini, A., Rosi, A., Mora, P., Zambonelli, F., & Ronchetti, F. (2010). LiDAR and hyperspectral data integration for landslide monitoring: The test case of Valoria landslide. *Italian Journal of Remote Sensing*, *42*(3), 89–99. https://doi.org/10.5721/itjrs20104237

Van Westen, C. J., & Lulie Getahun, F. (2003). Analyzing the evolution of the Tessina landslide using aerial photographs and digital elevation models. *Geomorphology*, *54*(1–2), 77–89. https://doi.org/10.1016/S0169-555X(03)00057-6

Van Westen, C. J., Rengers, N., & Soeters, R. (2003). Use of geomorphological information in indirect landslide susceptibility assessment. *Natural Hazards*, *30*, 399–419. https://doi.org/10.1023/B:NHAZ.0000007097.42735.9e